Author Manuscript

Author Manuscript

Author Manuscript

Author Manuscript

HHS Public Access

Author manuscript

Cell Rep. Author manuscript; available in PMC 2018 November 22.

Published in final edited form as:

Cell Rep. 2018 August 14; 24(7): 1713–1721.e4. doi:10.1016/j.celrep.2018.07.040.

Stress-Induced Low Complexity RNA Activates Physiological Amyloidogenesis

Miling Wang[1,2,3], **Xianzun Tao**[1,2], **Mathieu D. Jacob**[4], **Clayton A. Bennett**[1,2], **J.J. David Ho**[1,2], **Mark L. Gonzalgo**[2,3], **Timothy E. Audas**[5], and **Stephen Lee**[1,2,3,4,6,*]

[1]Department of Biochemistry and Molecular Biology, Miller School of Medicine, University of Miami, Miami, FL 33136, USA

[2]Sylvester Comprehensive Cancer Center, Miller School of Medicine, University of Miami, Miami, FL 33136, USA

[3]Department of Urology, Miller School of Medicine, University of Miami, Miami, FL 33136, USA

[4]Department of Cellular and Molecular Medicine, Faculty of Medicine, University of Ottawa, Ottawa, ON K1H 8M5, Canada

[5]Department of Molecular Biology and Biochemistry, Simon Fraser University, Burnaby, BC V5A 1S6, Canada

[6]Lead Contact

SUMMARY

Amyloid bodies (A-bodies) are inducible membraneless nuclear compartments composed of heterogeneous proteins that adopt an amyloid-like state. A-bodies are seeded by noncoding RNA derived from stimuli-specific loci of the rDNA intergenic spacer (rIGSRNA). This raises the question of how rIGSRNA recruits a large population of diverse proteins to confer A-body identity. Here, we show that long low-complexity dinucleotide repeats operate as the architectural determinants of rIGSRNA. On stimulus, clusters of rIGSRNA with simple cytosine/ uracil (CU) or adenosine/guanine (AG) repeats spanning hundreds of nucleotides accumulate in the nucleolar area. The low-complexity sequences facilitate charge-based interactions with short cationic peptides to produce multiple nucleolar liquid-like foci. Local concentration of proteins with fibrillation propensity in these nucleolar foci induces the formation of an amyloidogenic liquid

This is an open access article under the CC BY-NC-ND license (http://creativecommons.org/licenses/by-nc-nd/4.0/).

*Correspondence: stephenlee@med.miami.edu.

AUTHOR CONTRIBUTIONS

M.W., X.T., M.D.J. (cell biology), and T.E.A. (electron microscopy) performed the experiments, with technical assistance from C.A.B. (cloning), and J.J.D.H. M.W., X.T., M.L.G., T.E.A., and S.L. conceived the experiments and analyzed the data. M.W., T.E.A., and S.L. wrote the paper.

DECLARATION OF INTERESTS

The authors declare no competing interests.

SUPPLEMENTAL INFORMATION

Supplemental Information includes four figures and one table and can be found with this article online at https://doi.org/10.1016/j.celrep.2018.07.040.

DATA AND SOFTWARE AVAILABILITY

The accession number for the RNA sequencing data reported in this paper is GEO: GSE115731 (https://www.ncbi.nlm.nih.gov/geo/query/acc.cgi?acc=GSE115731).

Author Manuscript Author Manuscript Author Manuscript Author Manuscript

phase that seeds Abodies. These results demonstrate the physiological importance of low-complexity RNA and repetitive regions of genomethe genome often dismissed as “junk” DNA.

In Brief

Wang et al. report the identification of stress-induced low-complexity ribosomal intergenic RNA that drive the formation of an amyloidogenic liquid-like phase. Concentration of proteins with fibrillation propensity by low-complexity RNA initiates an amyloidogenic program that confers A-body identity.

Graphical Abstract

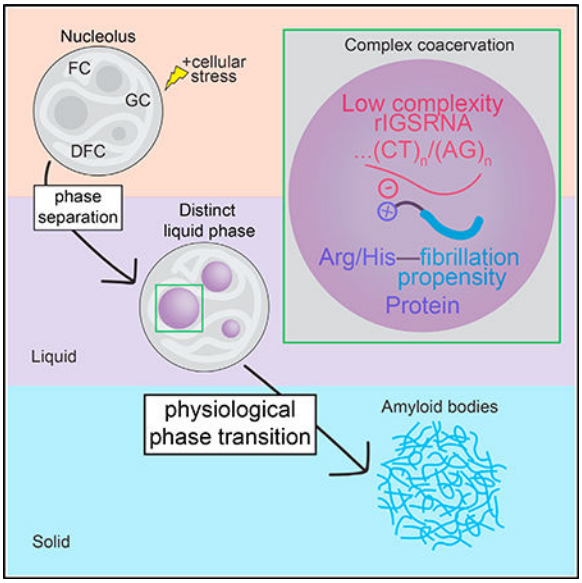

INTRODUCTION

In addition to membrane-bound organelles, eukaryotic cells contain numerous membrane-less compartments, also known as biomolecular condensates. The diversity of membrane-less compartments has expanded in recent years to include both dynamic and non-dynamic cellular bodies (Woodruff et al., 2018). Dynamic membrane-less bodies are liquid-like, as they are demixed (phase separated) from their surroundings, spherical, undergo cycles of fusion and fission, and their constituents exchange rapidly with the cellular milieu (Shin and Brangwynne, 2017; Woodruff et al., 2018). Cytoplasmic stress granules, processing bodies (P-bodies), nucleoli, and Cajal bodies are typical examples. In contrast, non-dynamic membrane-less bodies, such as centrosomes, Balbiani bodies, and nuclear amyloid bodies (A-bodies) are mostly composed of immobile proteins (Audas et al., 2016; Boke et al., 2016; Woodruff et al., 2018). In the cases of Balbiani bodies and A-bodies, their non-dynamic nature is attributed to proteins adopting a reversible amyloid-like conformation (Audas et al., 2016; Berchowitz et al., 2015; Boke et al., 2016; Fowler et al., 2006). Whereas dynamic assemblies concentrate relevant components for biochemical reactions (Banani et al., 2017), non-dynamic structures, such as A-bodies and Balbiani bodies, induce cellular dormancy

Author Manuscript Author Manuscript Author Manuscript Author Manuscript

(Audas et al., 2016; Boke et al., 2016; Wang et al., 2017). A-bodies are composed of an array of endogenous proteins and assemble in response to various cellular cues, including thermal stress and extracellular acidosis, and can be readily dissolved by the heat shock chaperone machinery (Audas et al., 2016). Hence, cells are equipped with systemic physiological amyloidogenic programs to regulate cellular states.

It remains a question what molecular and structural determinants confer the identity of cellular bodies. Although the focus has been on low-complexity sequences in intrinsically disordered regions of proteins (Banani et al., 2017; Shin and Brangwynne, 2017), several bodies use noncoding RNA (ncRNA) as the scaffolding molecule. Hirose and colleagues have neatly summarized the widespread use of architectural RNA in constructing membrane-less compartments (Chujo and Hirose, 2017; Chujo et al., 2017). This raises the question: what are the scaffolding elements embedded in these ncRNA that drive the formation of RNA-seeded cellular bodies? Assembly of A-bodies requires expression of long noncoding RNA derived from stimuli-specific loci of the rDNA intergenic spacer (rIGSRNA) (Audas et al., 2012, 2016). Much of the rDNA intergenic spacer consists of long simple dinucleotide (e.g., cytosine/thymine [CT] or adenosine/guanine [AG]) repetitive sequences that have historically been dismissed as useless “junk” DNA (Smirnov et al., 2016). Yet these long dinucleotide repeats are the only evolutionarily conserved regions between human and mouse rDNA intergenic spacer sequences. Therefore, we hypothesized that low-complexity sequences act as architectural determinants of rIGSRNA that activate a cell-wide amyloidogenic program to assemble A-bodies.

Here, we provide evidence that the simple dinucleotide repeats of the rDNA intergenic spacer are transcribed in response to stimuli that induce formation of A-bodies. The low-complexity rIGSRNA sequences interact with short cationic peptides to induce a distinct liquid-like phase in the nucleolar area. Concen-tration of proteins with fibrillation propensity in these foci seeds an amyloidogenic-like program that activates A-body biogenesis. We highlight the role of low-complexity RNA in constructing membrane-less compartments and the need to reassess the importance of genomic repetitive sequences.

RESULTS

rIGSRNA Contain Low-Complexity Sequences

We noticed that the human rDNA intergenic spacer is enriched in evolutionarily conserved long CT or AG dinucleotide repeats. These simple repeats are near positions ~16 kb and ~22 kb or ~28 kb downstream of the rRNA transcription start site, which are binding sites of A-body proteins in heat shock or acidosis, respectively (Figure 1A; Audas et al., 2012). RNA sequencing (RNA-seq) analyses and qPCR identified heat-shock-inducible transcripts between positions ~16 kb and ~23 kb of the rDNA intergenic spacer (Figures 1B, S1A for experimental schematic, and S1B). In keeping with previous nomenclature, we refer to these inducible RNA as $rIGS_{16}$RNA and $rIGS_{22}$RNA. Several heat-shock-inducible reads contained long CU or AG repeats flanked by non-repetitive sequences, which facilitated annotation to the rDNA intergenic spacer (Figure 1B). The read depth likely underestimated the expression of CU and AG repeats because RNA-seq products containing exclusively repetitive sequences are generally discarded prior to analyses. We also note that the read

Author Manuscript Author Manuscript Author Manuscript Author Manuscript

clusters may arise from any of the ~400 rDNA intergenic spacers and are not necessarily organized in tandem as depicted in Figure 1B. Clonal sequencing of heat-shock-inducible RT-PCR products confirmed that rIGSRNA contained long low-complexity sequences (Figures 1C and S1C). Hereafter, we refer to “low complexity” sequences as RNA containing long dinucleotide repeats predicted not to form secondary structures and “high complexity” sequences as RNA predicted to form secondary structures. Induction was also detected at position 18 kb of the rDNA intergenic spacer, but those transcripts did not contain repetitive sequences, nor did the region assemble with A-body proteins under heat shock (Figures 1A and1B; Audas et al., 2012). No heat-shock-inducible reads were observed downstream of position ~23 kb of the rDNA intergenic spacer, except for the rRNA transcription regulator pRNA (Figures 1B and S1B; Audas et al., 2012; Mayer et al., 2006).

Next, RNA-fluorescence in situ hybridization (FISH) was performed with probes specific to low-complexity sequences of rIGSRNA. These various probes only detected foci in nucleoli of heat-shocked cells (Figure 1D). RNA-FISH analysis also identified inducible foci of CU repeat-rich $rIGS_{28}$RNA in cells exposed to acidosis (Figures 1D and S1D for probe locations). Signal was specific to the stress condition (Figure S1E), and no signal was detected in untreated cells, in RNaseA-treated cells (Figure S1F), or in cells exposed to stressors that do not generate A-bodies (Figure S1G). Put together, these results suggest that clusters of rIGSRNA induced on stimuli contain low-complexity CU or AG repetitive sequences.

Low-Complexity rIGSRNAs Recruit A-Body Proteins to Distinct Nucleolar Foci

Time-lapse imaging revealed that A-body formation was a gradual process: A-body proteins, such as CDK1 and VHL fused to GFP, first formed multiple nucleolar foci on exposure to heat shock (Figure 2A) or extracellular acidosis (Figure S2A). The nucleolar foci were spherical, expanded in number (Figure 2B), fused (Figure S2B), and contained mobile proteins as assessed by photobleaching (Figures 2C, fluorescence recovery after photobleaching [FRAP] and fluorescence loss in photobleaching [FLIP], and S2C), all properties associated with dynamic, liquidlike, membrane-less compartments. These foci assembled outside the known phase-separated nucleolar compartments (Figure 2D; Feric et al., 2016; Hutten et al., 2011). With time, nucleolar foci fused to form large, non-dynamic A-bodies (Figures 2A and2C) that stained positive for Congo red (Figure S2D; Audas et al., 2016). Consistent with an architectural role, silencing of $rIGS_{16}$RNA and $rIGS_{22}$RNA delayed the recruitment of A-body proteins to the nucleolus, evidenced by the reduced number of liquid-like nucleolar foci, and impaired formation of mature A-bodies during heat shock (Figures 2E and S2E). Silencing of RNA from position ~18 kb of the rDNA intergenic spacer had no such effects, as expected (Figures 2E and S2E).

Next, we asked whether low-complexity sequences operate as architectural determinants of rIGSRNA involved in the recruitment of A-body proteins. Proteinase K (PK) digestion was essential to detect low-complexity rIGSRNA sequences with three RNA-FISH probes, demonstrating RNA hybridization was occluded by assembly of proteins on repetitive sequences (Figures 2F and S2F). In stark contrast, detection of two independent high-

Author Manuscript Author Manuscript Author Manuscript Author Manuscript

complexity rIGSRNA sequences by RNA-FISH (see Figure 1B for probe locations) did not require proteinase K digestion (Figures 2F and S2F).

We reasoned that an appropriate approach to compete with clusters of low-complexity RNA molecules would be with negatively charged nanoparticles (Nano$^-$), which are efficiently internalized and well tolerated by cells. Treatment with Nano$^-$ did not affect the production of rIGSRNA (Figure S2G). Interest-ingly, proteinase K digestion was not required to detect low-complexity rIGSRNA by RNA-FISH in Nano$^-$-treated cells, indicating that these negatively charged particles effectively competed with rIGSRNA and proteins assembly (Figure 2G). Likewise, treatment with Nano$^-$ impaired formation of VHLGFP nucleolar foci and mature A-bodies in thermal-stressed cells (Figure 2G) but did not affect formation of other cellular bodies (e.g., Cajal bodies, nucleoli, and nuclear and cytoplasmic stress granules; Figure S2H). Uncharged nanoparticles (Nano) had no observable effects (Figure 2G). These results suggest that nucleolar clusters of low-complexity rIGSRNA recruit proteins to liquid-like nucleolar foci to activate A-body formation.

Recruitment of Short Cationic Peptides by Low-Complexity rIGSRNAs

Next, we examined the mechanism by which low-complexity rIGSRNAs are able to recruit proteins to nucleolar foci. The amyloid-converting motif (ACM) is a β-amyloid-like motif that is necessary and sufficient to immobilize many proteins in A-bodies (Audas et al., 2016). The ACM of VHL (ACM^{VHL}) and β-amyloid(1–40), as well as the ACM of several other characterized A-body proteins, comprise a short cationic domain flanking a fibrillation propensity domain (Figures 3A and S3A; Goldschmidt et al., 2010). Reconstituted *in vitro*, mixing of 5'FAM labeled low-complexity RNA derived from rIGSRNA CU or AG repeats with unlabeled peptides containing the short cationic domain of ACM^{VHL} or β-amyloid resulted in numerous liquid droplets observable by differential interference contrast and fluorescence microscopy (Figures 3B and S3B). In contrast, two independent RNA derived from high-complexity regions of rIGSRNA failed to form droplets under identical conditions (Figures 3B and S3B). For these *in vitro* assays, RNA secondary structure was predicted by folding analyses and confirmed by absorbance at 260 nm (A_{260}) as a function of temperature (Figure S3C; Aumiller et al., 2016; Nott et al., 2016). *In vivo*, the short cationic domains of ACM^{VHL} or β-amyloid fused to GFP were recruited by rIGSRNA in nucleolar foci of cells exposed to heat shock (Figure 3C). Increasing salt concentration from 150 mM to 250 mM was sufficient to rapidly dissolve the droplets *in vitro* and nucleolar foci *in vivo*, suggesting a role for electrostatic interactions between short cationic domains and low-complexity rIGSRNA (Figure 3D; Altmeyer et al., 2015; Lin et al., 2015; Nott et al., 2015; Patel et al., 2015). Consistent with these results, the ACM^{VHL} was not efficiently captured by A-bodies when the arginine and histidine residues were substituted to aspartic acid (Figures S3D and S3E).

To further demonstrate that low-complexity rIGSRNAs are particularly efficient at interacting with short cationic peptides by electrostatic interactions, we produced GFP fusion proteins with three or four positively charged arginine residues (R^3-GFP and R^4-GFP). Similar to the ACM short cationic domain, R^3-GFP and R^4-GFP were diffuse in untreated cells and only responsive to conditions that induced expression of rIGSRNA

Author Manuscript Author Manuscript Author Manuscript Author Manuscript

(Figures 3E, S3F, and S3G). GFP fusion to aspartic acid (D^4-GFP) was unresponsive to all tested stressors (Figures 3E and S3G). *In vitro*, R^4 peptide formed droplets in the presence of low-, but not high-, complexity rIGSRNA (Figure 3E). Increasing [NaCl] to 250 mM was sufficient to rapidly dissolve R^4-GFP nucleolar foci and R^4 peptide droplets *in vivo* and *in vitro* (Figures 3F and S3H). Hence, low-complexity rIGSRNAs efficiently recruit proteins in nucleolar foci by processes that include charge-based interactions with short cationic domains.

Low-Complexity rIGSRNA-Seeded Amyloidogenic Liquid Phase Confers A-Body Identity

β-amyloid(1–40)-GFP formed nucleolar foci prior to immobilization (Figure 4A, top row). The short cationic domain of β-amyloid alone was recruited in nucleolar foci early in heat shock but failed to incorporate into mature A-bodies without a fibrillation propensity domain (Figures S3A and 4A, bottom row) or with a mutated (i.e., LMV → QTN) non-functional fibrillation propensity domain (Figure 4B). This was particularly evident when artificial R^4-GFP was fused to the β-amyloid fibrillation propensity domain (β-amyloid(17–40); also known in the literature as P3; R^4-P3-GFP). Whereas R^4-GFP returned to its original subcellular localization during late heat shock, R^4-P3-GFP was immobilized in A-bodies, in a rIGSRNA-dependent manner (Figures S4A and S4B). The fibrillation propensity domain alone failed to be recruited in nucleolar foci or be incorporated in mature A-bodies (Figure S4C). Principles of *in vitro* amyloidogenesis dictate that the amyloid state is favored at high concentration of polypeptides (Knowles et al., 2014). Accordingly, we suspected that short cationic domains concentrate fibrillation propensity domains in nucleolar foci to activate amyloidogenic processes. Consistent with this model, we noticed the appearance of rIGSRNA-dependent electron-dense material with the concomitant loss of the distinctive nucleolar organization during early acidosis (Figures 4C and S4D). In addition, staining with antibody A11 and the dye 8-anilino-1-naphthalenesulfonic acid (ANS) that detect oligomers and pre-fibril structures *in vitro* revealed the presence of pre-amyloid structures in cells exposed to heat shock and acidosis (Figures 4D and S4E), but not to other stressors (Figures S4F and S4G; Kayed et al., 2007). We referred to these structures as “nascent” A-bodies.

In vitro aggregation and kinetic models of amyloidogenesis predict that, once seeded, fibril growth occurs rapidly by propagation of the amyloid fold (Eisenberg and Jucker, 2012; Kelly, 2000; Knowles et al., 2014). In agreement with these *in vitro* models, expansion of nascent A-bodies occurred rapidly after a lag phase (Figure 4E). FLIP analyses during the expansion phase (e.g., 45’ heat shock) identified two β-amyloid(1–40)GFP populations in a cell: an abundant highly mobile diffuse pool and a discrete immobile pool in nascent A-bodies (Figures 4F and S4H). The pool of β-amyloid(1–40)-GFP in nascent A-bodies identified as immobile by FLIP showed partial recovery by FRAP analyses (Figures 4F and S4H). These experiments suggest that, once seeded, nascent A-bodies expand autonomously by the continuous addition and immobilization of mobile proteins in an amyloidogenic propagation-like process (diagram in Figure 4F). The expansion of nascent A-bodies terminated after the mobile pool of proteins was depleted (Figures 2A and S4H) and correlated with fibers of mature A-bodies observable by electron microscopy (Figure 4C). These results demonstrate that rIGSRNA concentrate proteins in nucleolar foci to activate an amyloidogenic-like process that drives A-body biogenesis.

Author Manuscript Author Manuscript Author Manuscript Author Manuscript

DISCUSSION

This study presents evidence supporting a role for inducible long low-complexity RNA in the formation of non-dynamic, solid-like, nuclear compartments called A-bodies. We propose a model whereby rIGSRNAs form clusters of low-complexity RNA in the nucleolus that efficiently induce multiple liquid-like foci with short cationic peptidedomains. This process is likely driven bycomplex coacervation, a form of liquid-liquid phase separation, which has been observed in other settings *in vivo* (Pak et al., 2016). Proteins with fibrillation propensity concentrated in these foci initiate an amyloidogenic process to form nascent A-bodies. Once seeded, nascent A-bodies self-assemble by directly immobilizing proteins via an amyloidogenic propagation-like pathway. As such, A-body biogenesis may represent a physiological liquid-to-solid phase transition, a process typically associated with pathological solid aggregate formation (Patel et al., 2015; Peskett et al., 2018; Posey et al., 2018). This study highlights the importance of long lowcomplexity RNA in constructing membrane-less compartments in a cell, adding to the list of architectural determinants of liquid droplets, which includes low-complexity protein domains, sequence-specific RNA, and short unstructured RNA *in vitro* (Jain and Vale, 2017; Kato et al., 2012; Nott et al., 2016; Shin and Brangwynne, 2017). More broadly, the data suggest we reassess the importance of different simple repeats (Caudron-Herger et al., 2015; Lubelsky and Ulitsky, 2018) commonly observed throughout the genome and often dismissed as useless DNA.

It has been suggested that the random coil state of RNA provides greater accessibility for binding of short cationic molecules than structured RNA (Aumiller et al., 2016). This might explain why proteins with short cationic domains, such as the ACM and artificial R^4-GFP described in this study, are particularly sensitive to expression of low-complexity rIGSRNA *in vivo*. It is possible that proteins with long cationic motifs (Mitrea et al., 2016) often observed in intrinsically disordered domains interact with rIGSRNA. Regardless, once recruited by rIGSRNA, only proteins with fibrillation propensity domains will be immobilized and incorporated into A-bodies. It is these properties (i.e., short cationic domain near a fibrillation propensity domain) that confer A-body identity and differentiate the ACM from other motifs associated with various phase-separated cellular bodies. The level of expression of low-complexity rIGSRNA, suggested by our RNA-FISH results, is likely sufficient to concentrate proteins with ACM to activate an amyloidogenic process. Whereas other low-complexity RNAsexist in cells, theymayspecifically recruit proteins (e.g., polyadenylated RNA and poly(A) binding proteins) or may not be expressed and/or clustered sufficiently to concentrate proteins and initiate amyloidogenesis. As such, the formation of A-bodies represents a cellular example of concentration-dependent activation of protein fibrillation observed in various *in vitro* assays for the past 40 years (Eisenberg and Jucker, 2012; Knowles et al., 2014).

The study of the rDNA intergenic spacer posed many unique challenges. The presence of more than 400 heterogeneous units complicates our ability to annotate variants of rIGSRNA in terms of length, abundance, and transcriptional start and stop sites. Despite these challenges, the discovery of low-complexity rIGSRNAs that induce physiological amyloidogenesis highlights the importance of characterizing this enigmatic region of the human genome. The data compel us to reassess the significance of low-complexity

Author Manuscript Author Manuscript Author Manuscript Author Manuscript

sequences in the genome that are often masked in databanks, currently discarded by RNA-seq technology, and largely ignored. It will be interesting to see how different charged residues (i.e., R, H, or K), their positioning in proteins, and the arrangement of low-complexity dinucleotide repeats drive condensate identity. Whether aberrant production or localization of low-complexity RNA is involved in amyloid pathologies, such as Alzheimer's and Huntington's diseases, remains the subject of future studies.

STAR★METHODS

KEY RESOURCES TABLE

Author Manuscript Author Manuscript Author Manuscript Author Manuscript

REAGENT or RESOURCE	SOURCE	IDENTIFIER
Antibodies		
Rabbit polyclonal anti-A11	Abcam	Cat# ab126892; RRID: AB_11128526
Rabbit polyclonal anti-CDK1	Abcam	Cat# ab133327; RRID: AB_11155333
Sheep anti-DIG-Rhodamine, fab fragments	Sigma	Cat# 11207750910; RRID: AB_514501
Goat anti-rabbit AlexaFluor 488/555	ThermoFisher Scientific	Cat# A-11008/A-21428; RRID: AB_143165/ RRID: AB_141784
Chemicals, Peptides, and Recombinant Proteins		
Congo red	Sigma	75768
ANS	Sigma	A1028
Proteinase K, molecular biology grade	New England BioLabs	P8107S
1.4nm Nanogold negatively charged nanoparticles	Nanoprobes	2023
1.4nm Nanogold neutral nanoparticles	Nanoprobes	2010
ACM^{VHL} Short cationic domain: GTGRRIHSYRGHLWLF	This paper	N/A
β-amyloid Short cationic domain: DAEFRHDSGYEVHHQKL	This paper	N/A
ACM^{VHL} Short cationic domain – D mutant: GTGDDIHSYDGHLWLF	This paper	N/A
β-amyloid Short cationic domain – D mutant: DAEFDDDSGYEVDDQDL	This paper	N/A
R^4: RRRR	This paper	N/A
Critical Commercial Assays		
TRIzol	ThermoFisher Scientific	15596018
High-Capacity cDNA Reverse Transcription Kit	Applied Biosystems	4368814
PowerUp SYBR Green master mix	Applied Biosystems	A25780
pGEM-T Easy vector system	Promega	A1360
Illumina NextSeq 500 High Output kit	Illumina	FC-404–2004
Deposited Data		
Raw and analyzed data	This paper	GSE115731
Human reference genome NCBI Build 38, GRCh38	Genome Reference Consortium	https://www.ncbi.nlm.nih.gov/projects/genome/assembly/grc/hu
U13369 human ribosomal DNA unit	Pubmed	https://www.ncbi.nlm.nih.gov/nuccore/555853/
GL000220.1 human ribosomal DNA unit from GRCh38	Genome Reference Consortium	https://www.ncbi.nlm.nih.gov/projects/genome/assembly/grc/hu
BK000964.3 mouse ribosomal DNA unit	Pubmed	https://www.ncbi.nlm.nih.gov/nuccore/bk000964
Experimental Models: Cell Lines		
Human: MCF7 breast cancer cell line	ATCC	HTB-22
Oligonucleotides		
Primers for qPCR, see Table S1	This paper	N/A
RNA-FISH HC sequences, see Table S1	This paper	N/A
RNA-FISH $rIGS_{16}$RNA LC: 5'-DIG-AGGAA	This paper	N/A

Author Manuscript Author Manuscript Author Manuscript Author Manuscript

REAGENT or RESOURCE	SOURCE	IDENTIFIER
GGAGGGAAGGAAGGAAGGAAGGAAGG AAGGAAGGAAGGAAATAAA-DIG-3’		
RNA-FISH rIGS$_{22}$RNA LC1: 5’-DIG-TTTTC TTTCATTTTCTCTTTCTTTTCTTTTCTTTT TTTCTTTCTTGTATA-DIG-3’	This paper	N/A
RNA-FISH rIGS$_{22}$RNA LC2: 5’-DIG- ACAC AGAGAGAAAGACAGAGACGAACAGAGA GAAACAGACAGAGAGAAGG-DIG-3’	This paper	N/A
siRNA target sequences, see Table S1	This paper	N/A
In vitro RNA low complexity CU: 5’- UCUG UCUCUGUCUUUGUCUCUCUCUCCCC UCUCUGCCUGUCUCACUGUGUCUGUC UUCUGUCUUACUCUCUUUCUCUCCCC GUCUGUCUCUCUCUCUCU-3’	This paper	N/A
In vitro RNA low complexity AG: 5’-AGAGAG AGAGACAGAGAGAGACAGAGAGAGAGAGA GAGGAGGGAGAGAGAAAAAAGAAAGAAAA AAAGAAAAGAAAAGAAAGAGAAAAUGAAA GAAAAGG-3’	This paper	N/A
In vitro RNA high complexity #1: 5’-CCGGGAUUU CAGCCUUUAAAAGCGCGGGCCCUGCCACCUUU CGCUGUGGCCCUUACGCUCAGAAUGACGUGU CCUCUCUGCCGUAGGUUGACUCCUUGAG-3’	This paper	N/A
In vitro RNA high complexity #2: 5’-CCGGCCCGCC UGGUCUUCUGUCUCUGCGCUCUGGUGACCUCA GCCUCCCAAAUAGCUGGGACUACAGGGAUCUCU UAAGCCCGGGAGGGAGAGGUUAACG-3’	This paper	N/A
Recombinant DNA		
Plasmid: pFLAG-GFP	Audas et al., 2016	N/A
Plasmid: pEGFP-N1 TOPO™ Expression kit	ThermoFisher Scientific	K481001
Plasmid: pEGFP-C1 TOPO™ Expression kit	ThermoFisher Scientific	K482001
Software and Algorithms		
RNAfold		http://rna.tbi.univie.ac.at/cgi-bin/RNAWebSuite/RNAfold.cgi
ZipperDB for fibrillation propensity	Goldschmidt et al., 2010	https://services.mbi.ucla.edu/zipperdb/
Cutadapt (v1.15)		https://github.com/marcelm/cutadapt/
STAR (v2.3)		https://github.com/alexdobin/STAR
Samtools		http://samtools.sourceforge.net/
Integrative Genomics Viewer		http://software.broadinstitute.org/software/igv/

CONTACT FOR REAGENT AND RESOURCE SHARING

Further information and requests for reagents may be directed to, and will be fulfilled by the corresponding author, Dr. Stephen Lee (stephenlee@med.miami.edu).

EXPERIMENTAL MODEL AND SUBJECT DETAILS

MCF-7 cells, derived from female mammary gland adenocarcinoma tissue, were purchased from the ATCC (HTB-22) and grown in DMEM (high glucose) supplemented with 10% Fetal Bovine Serum (FBS) and 1% penicillin-streptomycin. Cells were maintained under standard growth conditions: 37°C and 5% CO_2 in a humidified atmosphere. Heat shock was at 43°C for the indicated times. Acidosis was at pH 6.0 in 1% O_2 (hypoxia). Hypoxia was

Author Manuscript Author Manuscript Author Manuscript Author Manuscript

induced by incubating cells in an H35 HypoOxystation at 37°C in a 1% O_2, 5% CO_2 and N_2-balanced environment. Sodium arsenite (125 mM), H_2O_2 (300 nM) and thapsigargin (300 nM), were used for the indicated times. 1.4nm Nanogold® negatively charged nanoparticles (Nanoprobes, #2023) or neutral nanoparticles (Nanoprobes, #2010) were directly added to the medium at 300 μM.

METHOD DETAILS

Detection of low complexity rIGSRNA transcripts—RNA from the digitonin-insoluble fraction (digitonin used at 40 μg/ml in PBS, on ice for 5 min) of MCF-7 cells was extracted with TRIzol (Thermo Fisher Scientific, 15596018) for QPCR, RT-PCR and RNA sequencing. **RT-PCR** was performed with 1 mg RNA input. Samples were first DNaseI treated (Promega) and heat inactivated for 10 min at 65°C before RT with the High Capacity cDNA Reverse Transcription kit (Applied Biosystems), according to manufacturer's protocol. Quantitative PCR (**QPCR**) was performed using PowerUp SYBR Green master mix (Applied Biosystems) on the ABI StepOne System (Thermo Fisher Scientific) with the indicated primers in Table S1. Unique primers were used to generate RT-PCR products that were gel extracted (QIAGEN) and cloned into the pGEM-T Easy vector (Promega). Sequencing services were provided by Genewiz. **RNA sequencing** was done on pooled RNA extractions to yield a no treatment sample and 30-min heat shock sample. The concentration and quality of the RNA was determined on a Qubit fluorometer (Thermo Fisher Scientific) and Bioanalyzer system (Agilent Technologies). Strand-specific libraries were prepared using the TruSeq Total RNA kit (Illumina). Ribosomal RNA was not depleted to prevent loss of expressed rIGSRNA transcripts. Sequencing of 150-base-pair paired-end reads was run using the Illumina NextSeq 500 High Output kit (300-cycles; 400M flow cell) at the Onco-Genomics Core Facility, Sylvester Cancer Center, University of Miami, USA. Reads were qualitycontrolled with Cutadapt. Reads were first mapped to rRNA sequences and discarded. The remaining "unmapped" reads were realigned with STAR on the human genome GRCh38 (2016) assembly, using non-default parameters to obtain a greater number of uniquely mapped reads. For the graphical representation of the RNA-seq data, base coverage profiles of GL000220.1, an unplaced contig containing an entire ribosomal cassette, were produced in Integrative Genomics Viewer. Expression levels were normalized to account for fewer input reads in the 30 min heat shock sample (after rRNA sequences were discarded). Forward strand reads were separated according to the SAM flags with a bash script. Reads that fell within Alu elements, their locations were obtained from the UCSC Browser, were filtered out after alignment. ***In situ* hybridization** was carried out with 5' and 3' digoxigenin (DIG)-labeled oligonucleotides. Post-fixation of 30', cells were quenched with 0.1M Tris-HCl, pH 7.0 for 10' before ± Proteinase K (PK) treatment (NEB, 800U/ml stock, 100,000× dilution) at 37°C for 30'. PK treatment was followed by a 5' 1% formaldehyde post-fix. RNaseA was used at 50 mg/ml for 30', 37°C. Cells were equilibrated in 2× SSC before O/N hybridization at 37°C. Probes (5pmol) were denatured at 85C for 10'. Hybridization buffer was 15% formamide, 10% dextran sulfate, 2mM vanadyl ribonucleoside and 2× SSC. Probes were detected with an anti-DIG-Rhodamine antibody (Sigma, 11207750910) at 20 mg/ml in 4× SSC. Slides were mounted in 90% glycerol.

Author Manuscript Author Manuscript Author Manuscript Author Manuscript

Plasmids and transfection protocol—VHL, CDK1, β-amyloid(1–40), short cationic domains of ACM^{VHL} and β-amyloid, fibrillation propensity domain of ACM^{VHL} and β-amyloid, rACM^{VHL}, rACM^{POLD1} in pFLAG-GFP, mCherry-VHL and RPA40, fibrillarin, B23, coilin, TIA1, HSF1 in pEGFP-N1 were previously generated (Audas et al., 2016; Jacob et al., 2013). R^3, R^4, D^4, R^3-P3, R^4-P3, D^4-P3, in pEGFP-C1 and all aspartic acid substitutions were generated by Genscript. Plasmids were transfected using Lipofectamine 3000 (Thermo Fisher Scientific) according to the manufacturer's protocol and treated/visualized/harvested 24h post-transfection. For siRNAs (100 pmol), cells were reverse-transfected using RNAiMAX (Thermo Fisher Scientific) and treated/harvested 48h post-transfection.

Congo red, ANS and A11 staining—Congo red (0.05%) was used as previously described (Audas et al., 2016) and mounted in 5% glycerol. ANS (Sigma, A1028) was used to detect denatured, hydrophobic protein structures. ANS was dissolved in DMSO for a 10mM stock solution. Post-fixation and permeabilization, it was used at 250 mM in PBS for 1 h with 1× wash in PBS before mounting in Fluoromount (Sigma). Polyclonal antibody A11 (Abcam, ab126892) was used to detect amyloid oligomers. Post-fixation for 30 min, cells were quenched with 0.1M Tris-HCl, pH 7.0 for 10 min before Proteinase K (PK) treatment (NEB, 800U/ml stock, 100,000× dilution) at 37°C for 30 min. PK treatment was followed by a 5-min 1% formaldehyde post-fix. Cells were blocked for 30 min with 5% horse serum in PBS followed by incubation with primary antibody rabbit anti-A11 (1:100) for 1 h at 37°C. After washing, cells were incubated for 1h, 37°C with goat anti-rabbit conjugated to AlexaFluor 555 (Molecular Probes, 1:500). The coverslips were mounted with Fluoromount.

Endogenous CDK1 staining—Cells were fixed in 1% formaldehyde for 10 min and permeabilized in 0.5% Triton X-100 for 5 min. Rabbit anti-CDK1 (Abcam, ab133327) was used at 1:500. After washing, cells were incubated for 1h, 37°C with goat anti-rabbit conjugated to AlexaFluor 488 (Molecular Probes, 1:500). The coverslips were mounted with Fluoromount.

***In vitro* droplet formation—**Untagged peptides were custom synthesized by GenScript (New Jersey, USA) at > 95% purity. Peptide stock solutions were kept at 50mM in nuclease-free-water. 5'-FAM labeled RNA were synthesized by Integrated DNA Technologies (IDT, Coralville IA) and resuspended in 50mM NaCl to 100 μM. 1 μM low or high complexity rIGSRNA was mixed with indicated peptide concentrations in 150mM NaCl and imaged after a 10' incubation.

Estimation of RNA secondary structure—The RNAfold webserver was used to predict RNA secondary structures, based on minimum free energy. Changes in RNA secondary structure were monitored through UV/Vis spectroscopy on the BMG LABTECH FLUOstar Omega. Aliquots of low complexity or high complexity RNA were heated along a temperature gradient and measured at 260nm and converted to normalized absorbance (norm. A_{260}).

Author Manuscript Author Manuscript Author Manuscript Author Manuscript

Fluorescence microscopy and image processing/analysis—For live imaging, cells were seeded in 145 μm 35mm glass-bottom plates. For fixed samples, cells were seeded in 35mm plates with no 1.5 glass coverslips. Cells were fixed in 4% formaldehyde for 10 min and permeabilized in 0.5% Triton X-100 for 5 min. Live cell images were captured by confocal microscopy (Leica TCS SP5; Leica Microsystems, Mannheim, Germany), fitted with a variable temperature and 5% CO_2 environmental chamber (Okolab), using a 63× Plan-Apochromat/1.4 NA oil immersion objective. Fixed slides were imaged on a Zeiss AxioObserver D1 microscope using a 63× Plan-Apochromat/1.4 NA objective. Excitation wavelengths were 405/410–450 nm for ANS, 488 nm/509–529 nm for GFP, AlexaFluor 488 and 5'FAM-RNA, and 555 nm/569–589 nm for AlexaFluor 555, mCherry, Congo red and anti-DIG-Rhodamine. Images, especially those with ANS, Congo Red and RNA-FISH, were uniformly adjusted to increase brightness/contrast while pseudo-coloring was achieved with the Hue/Saturation slider in Photoshop CC (Adobe). LUT coloration was done in ImageJ.

Photobleaching of GFP constructs—Live cells expressing GFP constructs of interest were seeded in 35mm glass-bottom plates and visualized on the DeltaVision Elite (GE Healthcare) in a 37C and 5% CO_2 environmental chamber using a 60× Silicone Plan-Apo/1.3 NA objective. The system was controlled by the Elite Master Workstation for bleaching and image acquisition. Photobleaching was performed with a 1 s 10% laser (488nm) power, 10 mW bleachpoint. For FLIP, the bleach point was subject to continuous bleaching at 6 s intervals for a total of 180 s. For FRAP, five pre-bleach measurements were taken before photobleaching and images were taken at 3.5 s intervals for a total of 180 s during recovery. Region intensity measurements were made in ImageJ and normalized as previously described in (Mekhail et al., 2005). All photobleaching graphs represent the average of at least 5 cells.

Nucleolar intensity—Normalized nucleolar intensity = average of (nucleolar fluorescence intensity/nuclear fluorescence intensity). Calculations were based on pixel intensity measurements made in ImageJ. Salt experiments were performed on living cells. 0.45 μm syringe filtered sodium chloride (NaCl) was added directly to the medium at the indicated concentrations and immediately imaged.

Fibrillation propensity—Rosetta free energy scores for proteins were calculated using online ZipperDB software (UCLA).

Transmission electron microscopy—2% glutaraldehyde fixed cells were washed and post-fixed in 1% osmium tetroxide. Samples were dehydrated in a series of ascending alcohols then embedded in Spurr's epoxy resin onto BEEM (West Chester, PA) capsule molds. Specimen blocks were ultrathin sectioned on a Leica EM UC6 ultramicrotome (Leica, Wetzlar, Germany), after which the sections were stained with uranyl acetate and lead citrate. Imaging occurred on a JEOL 1230 transmission electron microscope (Joel, MA).

Author Manuscript Author Manuscript Author Manuscript Author Manuscript

QUANTIFICATION AND STATISTICAL ANALYSIS

Graphs represent mean values. Error bars represent standard error of the mean (SEM) from three biological replicates. The p values were based on two-tailed Student's t test with the significance level indicated in the figure legends.

Supplementary Material

Refer to Web version on PubMed Central for supplementary material.

ACKNOWLEDGMENTS

We thank Megumi Ikegami for expert technical assistance, M.L. Bates at the Miami Project to Cure Paralysis for assistance with the TEM, and M. Boulina at the Analytical Imaging Core Facility of the Sylvester Comprehensive Cancer Center for assistance with the live-cell imaging. Research in this publication was supported by grants from the National Institute of General Medical Sciences (R01GM115342; S.L.) and the National Cancer Institute (R01CA200676) of the NIH, the Sylvester Comprehensive Cancer Center (S.L. and M.L.G.), and the Canadian Institutes of Health Research (CIHR) (15389; S.L.).

REFERENCES

Altmeyer M, Neelsen KJ, Teloni F, Pozdnyakova I, Pellegrino S, Grøfte M, Rask MB, Streicher W, Jungmichel S, Nielsen ML, and Lukas J (2015). Liquid demixing of intrinsically disordered proteins is seeded by poly(ADP-ribose). Nat. Commun 6, 8088. [PubMed: 26286827]

Audas TE, Jacob MD, and Lee S (2012). Immobilization of proteins in the nucleolus by ribosomal intergenic spacer noncoding RNA. Mol. Cell 45, 147–157. [PubMed: 22284675]

Audas TE, Audas DE, Jacob MD, Ho JJ, Khacho M, Wang M, Perera JK, Gardiner C, Bennett CA, Head T, et al. (2016). Adaptation to stressors by systemic protein amyloidogenesis. Dev. Cell 39, 155–168. [PubMed: 27720612]

Aumiller WM, Jr., Pir Cakmak F, Davis BW, and Keating CD (2016). RNA-based coacervates as a model for membraneless organelles: formation, properties, and interfacial liposome assembly. Langmuir 32, 10042–10053. [PubMed: 27599198]

Banani SF, Lee HO, Hyman AA, and Rosen MK (2017). Biomolecular condensates: organizers of cellular biochemistry. Nat. Rev. Mol. Cell Biol 18, 285–298. [PubMed: 28225081]

Berchowitz LE, Kabachinski G, Walker MR, Carlile TM, Gilbert WV, Schwartz TU, and Amon A (2015). Regulated formation of an amyloid-like translational repressor governs gametogenesis. Cell 163, 406–418. [PubMed: 26411291]

Boke E, Ruer M, Wühr M, Coughlin M, Lemaitre R, Gygi SP, Alberti S, Drechsel D, Hyman AA, and Mitchison TJ (2016). Amyloid-like self-assembly of a cellular compartment. Cell 166, 637–650. [PubMed: 27471966]

Caudron-Herger M, Pankert T, Seiler J, Németh A, Voit R, Grummt I, and Rippe K (2015). Alu element-containing RNAs maintain nucleolar structure and function. EMBO J. 34, 2758–2774. [PubMed: 26464461]

Chujo T, and Hirose T (2017). Nuclear bodies built on architectural long noncoding RNAs: unifying principles of their construction and function. Mol. Cells 40, 889–896. [PubMed: 29276943]

Chujo T, Yamazaki T, Kawaguchi T, Kurosaka S, Takumi T, Nakagawa S, and Hirose T (2017). Unusual semi-extractability as a hallmark of nuclear body-associated architectural noncoding RNAs. EMBO J. 36, 1447–1462. [PubMed: 28404604]

Eisenberg D, and Jucker M (2012). The amyloid state of proteins in human diseases. Cell 148, 1188–1203. [PubMed: 22424229]

Feric M, Vaidya N, Harmon TS, Mitrea DM, Zhu L, Richardson TM, Kriwacki RW, Pappu RV, and Brangwynne CP (2016). Coexisting liquid phases underlie nucleolar subcompartments. Cell 165, 1686–1697. [PubMed: 27212236]

Author Manuscript Author Manuscript Author Manuscript Author Manuscript

Fowler DM,Koulov AV,Alory-Jost C,Marks MS,Balch WE,andKelly JW (2006). Functional amyloid formation within mammalian tissue. PLoS Biol. 4, e6. [PubMed: 16300414]

Goldschmidt L, Teng PK, Riek R, and Eisenberg D (2010). Identifying the amylome, proteins capable of forming amyloid-like fibrils. Proc. Natl. Acad. Sci. USA 107, 3487–3492. [PubMed: 20133726]

Hutten S, Prescott A, James J, Riesenberg S, Boulon S, Lam YW, and Lamond AI (2011). An intranucleolar body associated with rDNA. Chromosoma 120, 481–499. [PubMed: 21698343]

Jacob MD, Audas TE, Uniacke J, Trinkle-Mulcahy L, and Lee S (2013). Environmental cues induce a long noncoding RNA-dependent remodeling of the nucleolus. Mol. Biol. Cell 24, 2943–2953. [PubMed: 23904269]

Jain A, and Vale RD (2017). RNA phase transitions in repeat expansion disorders. Nature 546, 243–247. [PubMed: 28562589]

Kato M, Han TW, Xie S, Shi K, Du X, Wu LC, Mirzaei H, Goldsmith EJ, Longgood J, Pei J, et al. (2012). Cell-free formation of RNA granules: low complexity sequence domains form dynamic fibers within hydrogels. Cell 149, 753–767. [PubMed: 22579281]

Kayed R, Head E, Sarsoza F, Saing T, Cotman CW, Necula M, Margol L, Wu J, Breydo L, Thompson JL, et al. (2007). Fibril specific, conformation dependent antibodies recognize a generic epitope common to amyloid fibrils and fibrillar oligomers that is absent in prefibrillar oligomers. Mol. Neurodegener 2, 18. [PubMed: 17897471]

Kelly JW(2000).Mechanismsofamyloidogenesis.Nat. Struct. Biol 7, 824–826. [PubMed: 11017183]

Knowles TP, Vendruscolo M, and Dobson CM (2014). The amyloid state and its association with protein misfolding diseases. Nat. Rev. Mol. Cell Biol 15, 384–396. [PubMed: 24854788]

Lin Y, Protter DS, Rosen MK, and Parker R (2015). Formation and maturation of phase-separated liquid droplets by RNA-binding proteins. Mol. Cell 60, 208–219. [PubMed: 26412307]

Lubelsky Y, and Ulitsky I (2018). Sequences enriched in Alu repeats drive nuclear localization of long RNAs in human cells. Nature 555, 107–111. [PubMed: 29466324]

Mayer C, Schmitz KM, Li J, Grummt I, and Santoro R (2006). Intergenic transcripts regulate the epigenetic state of rRNA genes. Mol. Cell 22, 351–361. [PubMed: 16678107]

Mekhail K, Khacho M, Carrigan A, Hache RR, Gunaratnam L, and Lee S (2005). Regulation of ubiquitin ligase dynamics by the nucleolus. J. Cell Biol 170, 733–744. [PubMed: 16129783]

Mitrea DM, Cika JA, Guy CS, Ban D, Banerjee PR, Stanley CB, Nourse A, Deniz AA, and Kriwacki RW (2016). Nucleophosmin integrates within the nucleolus via multi-modal interactions with proteins displaying R-rich linear motifs and rRNA. eLife 5, e13571. [PubMed: 26836305]

Nott TJ, Petsalaki E, Farber P, Jervis D, Fussner E, Plochowietz A, Craggs TD, Bazett-Jones DP, Pawson T, Forman-Kay JD, and Baldwin AJ (2015). Phase transition of a disordered nuage protein generates environmentally responsive membraneless organelles. Mol. Cell 57, 936–947. [PubMed: 25747659]

Nott TJ, Craggs TD, and Baldwin AJ (2016). Membraneless organelles can melt nucleic acid duplexes and act as biomolecular filters. Nat. Chem 8, 569–575. [PubMed: 27219701]

Pak CW, Kosno M, Holehouse AS, Padrick SB, Mittal A, Ali R, Yunus AA, Liu DR, Pappu RV, and Rosen MK (2016). Sequence determinants of intracellular phase separation by complex coacervation of a disordered protein. Mol. Cell 63, 72–85. [PubMed: 27392146]

Patel A, Lee HO, Jawerth L, Maharana S, Jahnel M, Hein MY, Stoynov S, Mahamid J, Saha S, Franzmann TM, et al. (2015). A liquid-to-solid phase transition of the ALS protein FUS accelerated by disease mutation. Cell 162, 1066–1077. [PubMed: 26317470]

Peskett TR, Rau F, O'Driscoll J, Patani R, Lowe AR, and Saibil HR (2018). A liquid to solid phase transition underlying pathological Huntingtin Exon1 aggregation. Mol. Cell 70, 588–601.e6. [PubMed: 29754822]

Posey AE, Ruff KM, Harmon TS, Crick SL, Li A, Diamond MI, and Pappu RV (2018). Profilin reduces aggregation and phase separation of huntingtin N-terminal fragments by preferentially binding to soluble monomers and oligomers. J. Biol. Chem 293, 3734–3746. [PubMed: 29358329]

Shin Y, and Brangwynne CP (2017). Liquid phase condensation in cell physiology and disease. Science 357, eaaf4382. [PubMed: 28935776]

Smirnov E, Cmarko D, Mazel T, Hornáček M, and Raška I (2016). Nucleolar DNA: the host and the guests. Histochem. Cell Biol 145, 359–372. [PubMed: 26847178]

Author Manuscript Author Manuscript Author Manuscript Author Manuscript

Wang M, Audas TE, and Lee S (2017). Disentangling a bad reputation: changing perceptions of amyloids. Trends Cell Biol 27, 465–467. [PubMed: 28359692]

Woodruff JB, Hyman AA, and Boke E (2018). Organization and function of non-dynamic biomolecular condensates. Trends Biochem. Sci 43, 81–94. [PubMed: 29258725]

Author Manuscript Author Manuscript Author Manuscript Author Manuscript

Highlights

- Stressors induce low-complexity RNA from “junk” repeats of the rDNA intergenic spacer
- Nucleolar low-complexity RNA initiates an amyloidogenic liquid phase
- Self-assembly of amyloidogenic proteins drives amyloid bodies
- Dinucleotide repeats are functional elements of noncoding RNA

Author Manuscript Author Manuscript Author Manuscript Author Manuscript

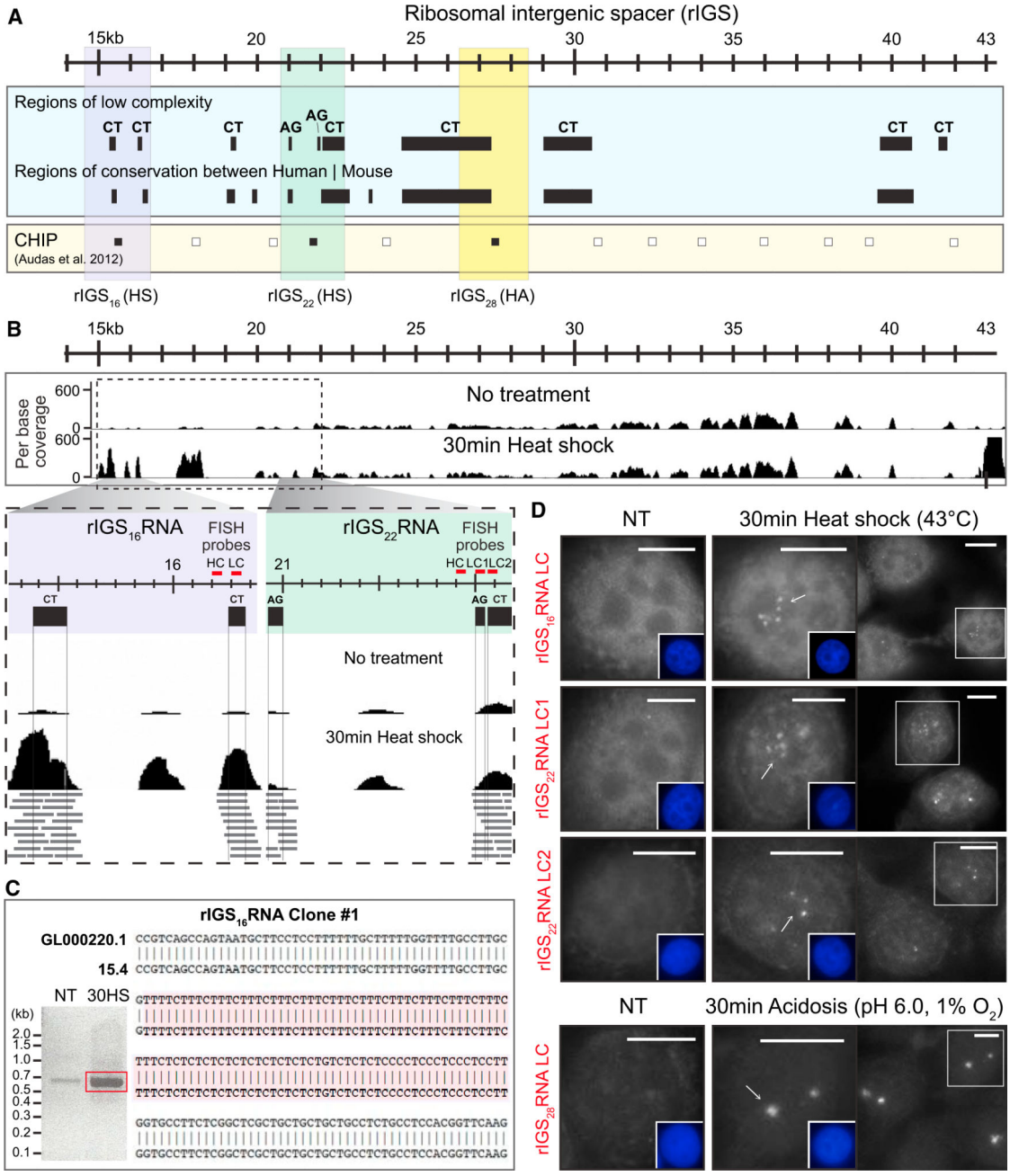

Figure 1. rIGSRNAs Contain Low-Complexity Sequences

(A) The human rIGS contains regions of evolutionarily conserved low-complexity sequences. Regions of conservation between human (supercontig U13369) and mouse (BK000964.3) rIGS include long low-complexity CT or AG repeats that flank A-body binding sites (black squares; Audas et al., 2012), from which $rIGS_{16}$RNA and $rIGS_{22}$RNA, in cells exposed to heat shock (HS), or $rIGS_{28}$RNA, in extracellular acidosis (HA), are induced.

(B–D) Strategies used to demonstrate expression and localization of low-complexity rIGSRNA transcripts at 30’ heat shock (43°C) or 30’ acidosis (pH 6.0; 1% O_2). (B) RNA-

Author Manuscript Author Manuscript Author Manuscript Author Manuscript

seq performed in MCF-7 cells revealed induction between 16 and 23 kb of the rIGS (GL000220.1) at 30’ heat shock. Reads (gray) containing low-complexity (LC) sequences from $rIGS_{16}$RNA and $rIGS_{22}$RNA were flanked by high-complexity (HC) sequences; (C) clonal sequence of an RT-PCR product (red box) that contained a long low-complexity sequence (highlighted in red); and (D) RNA-FISH with low-complexity probes. Hoechst marks nuclei (insets). The scale bars represent 10 μm.

Author Manuscript Author Manuscript Author Manuscript Author Manuscript

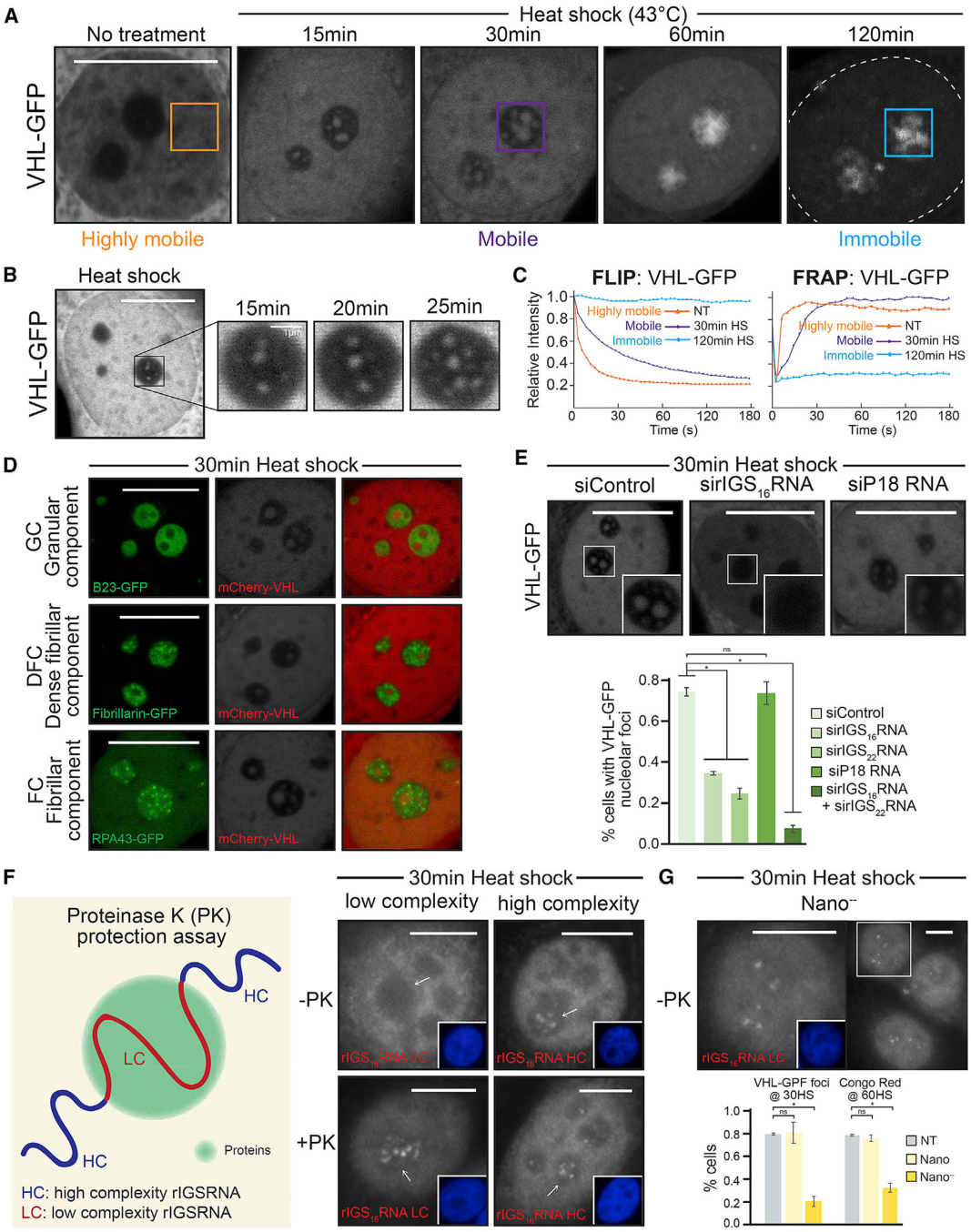

Figure 2. Low-Complexity rIGSRNAs Recruit A-Body Proteins to Liquid-like Nucleolar Foci

(A) Time-lapse images of a VHL-GFP-expressing cell exposed to heat shock (43°C). Squares refer to relative mobility of proteins as measured in Figure 2C. The scale bar represents 10 μm.

(B and C) Nucleolar foci of VHL-GFP displayed liquid-like properties. They were (B) spherical, expanded in number, and (C) contained mobile proteins (purple) as measured by fluorescence recovery after photobleaching (FRAP) and fluorescence loss in photobleaching (FLIP). Longer exposure to heat shock resulted in immobile proteins (blue).

Author Manuscript Author Manuscript Author Manuscript Author Manuscript

(D) Nucleolar foci of mCherry-VHL formed outside the known nucleolar compartments, marked by B23 (GC), fibrillarin (DFC), and RPA43 (FC), a subunit of RNA polymerase I.
(E) Formation of nucleolar foci at 30' heat shock was rIGSRNA dependent. Silencing of $rIGS_{16}$RNA (pictured), $rIGS_{22}$RNA, or both reduced the % of cells with VHL-GFP nucleolar foci. Silencing of P18 RNA had no effect. Graph represents means ± SEM. *$p < 0.05$, ns, not significant.
(F) Low-complexity rIGSRNA sequences were masked by proteins. The diagram and images depict PK digestion was required to visualize low-, but not high-,complexity $rIGS_{16}$RNA sequences by RNA-FISH at 30' heat shock. Hoechst marks nuclei (insets).
(G) Nano prevents capture of proteins by low-complexity rIGSRNA. Proteinase K digestion was not required to visualize low-complexity $rIGS_{16}$RNA by RNAFISH in cells treated with $Nano^-$. $Nano^-$, but not Nano, impaired the appearance of VHL-GFP nucleolar foci and mature A-bodies at 30' and 60' heat shock (HS), respectively. Hoechst marks nuclei. Graphs represent means ± SEM. *$p < 0.05$.
Unless otherwise denoted, scale bars represent 10 μm (B, D, E, and G).

Author Manuscript Author Manuscript Author Manuscript Author Manuscript

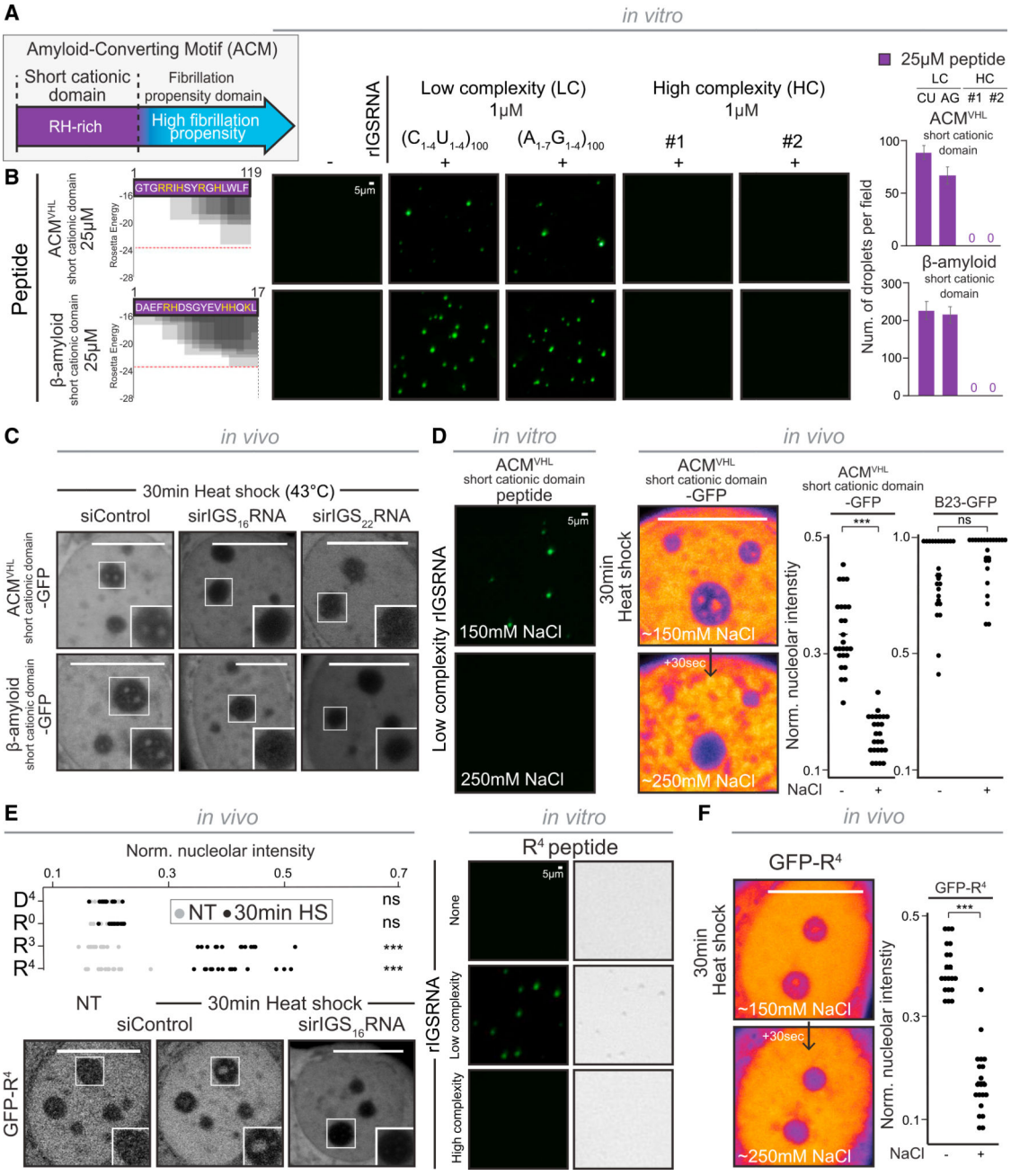

Figure 3. Recruitment of Short Cationic Peptides by Low-Complexity rIGSRNA

(A) The amyloid-converting motif (ACM) comprises of a short cationic domain flanking a fibrillation propensity domain.

(B) *In vitro*, 5'FAM-labeled RNA derived from rIGSRNA CU or AG low-complexity repeats phase separated with untagged peptides containing the short cationic domain of ACM^{VHL} or β-amyloid. Mixtures of high-complexity 5'FAM-labeled rIGSRNA and these peptides remained soluble. Graphs represent mean number of liquid droplets per field of view (n = 5) ± SEM.

(C) *In vivo*, GFP-tagged, short cationic domain of ACM^{VHL} or β-amyloid formed rIGSRNA-dependent nucleolar foci at 30^0 heat shock. The scale bars represent 10 μm.

Author Manuscript Author Manuscript Author Manuscript Author Manuscript

(D) Interactions between the short cationic domain of ACM^{VHL} or β-amyloid and low-complexity rIGSRNA were disrupted by salts. Increasing [NaCl] from 150 to 250 μM rapidly dissolved the liquid droplets and nucleolar foci at 30' heat shock *in vitro* and *in vivo*, respectively. Graph indicates loss of nucleolar intensity of GFP-tagged short cationic domain of ACM^{VHL} upon addition of salt (***$p < 0.001$). Addition of salt did not affect B23-GFP nucleolar intensity.

(E) Low-complexity rIGSRNAs recruit short cationic molecules. *In vivo*, arginine (R)-containing GFP-R^3 or GFP-R^4 was observed in nucleolar foci at 30' heat shock. GFP-R^4 is the typical example. Silencing of $rIGS_{16}$RNA prevented GFP-R^4 nucleolar foci. Graph represents the increase in nucleolar intensity of GFP-R^3 or GFP-R^4 compared to aspartic acid (D)-containing GFP-D^4 or R^0 (GFP alone). ***$p < 0.001$. *In vitro*, numerous liquid droplets were observed from mixture of R^4 peptide (250 μM) and low-, but not high-, complexity rIGSRNA.

(F) Formation of GFP-R^4 nucleolar foci was disrupted by salts. Increase of [NaCl] from 150 to 250 mM rapidly dissolved nucleolar foci at 30' heat shock. Graph represents loss of nucleolar intensity upon addition of salt. ***$p < 0.001$.

Unless otherwise denoted, scale bars represent 10 μm (D–F).

Author Manuscript Author Manuscript Author Manuscript Author Manuscript

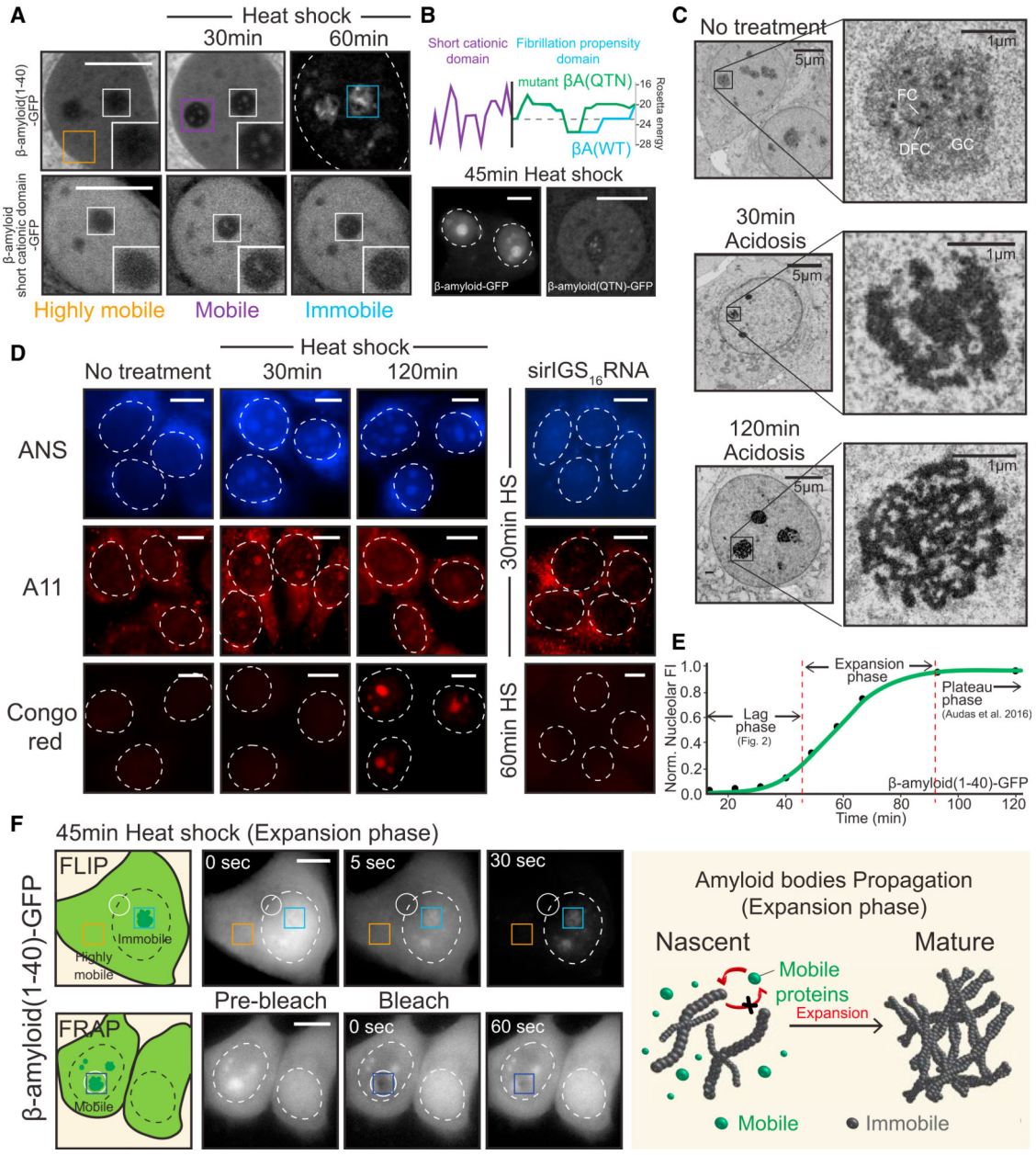

Figure 4. Low-Complexity rIGSRNA-Seeded A-Bodies Expand by Amyloidogenic-like Propagation

(A and B) Fibrillation propensity domain of the ACM determines A-body composition.

(A) GFP-tagged β-amyloid(1–40) formed nucleolar foci prior to immobilization in A-bodies (top row), whereas GFP-tagged short cationic domain of β-amyloid alone (without a fibrillation propensity domain; see Figure S3A) formed nucleolar foci but was not incorporated into A-bodies (bottom row).

(B) β-amyloid(1–40) with a LMV → QTN substitution, β-amyloid(QTN)-GFP, which has reduced fibrillation propensity, was not incorporated into mature A-bodies.

(C) The nucleolus was a site of concentration during extracellular acidosis (pH 6.0; 1% O_2). Transmission electron micrographs of amorphous electron-dense structures and then fibers

Author Manuscript Author Manuscript Author Manuscript Author Manuscript

in cells exposed to acidosis replaced intact nucleolar structures observed in untreated (NT) cells.

(D) Nascent A-bodies exhibit pre-amyloidogenic features. Nuclear ANS and A11 signals were present at 30^0 heat shock before Congo red was detected at 60'. Silencing of $rIGS_{16}$RNA prevented nuclear ANS, A11, and Congo red signals.

(E) Nucleolar intensity measurements of β-amyloid(1–40)-GFP in cells exposed to a heat shock time course revealed that, after an initial lag phase, nascent A-bodies undergo a rapid expansion phase and subsequent plateau phase.

(F) A-body expansion followed *in vitro* kinetic models of amyloid propagation. FLIP and FRAP analyses at 45' heat shock indicated nascent A-bodies autonomously expand through rapid addition and immobilization of mobile proteins to eventually form mature A-bodies. Bleach points are indicated by white circles.

Unless otherwise denoted, scale bars represent 10 μm (A–D and F).

Author Manuscript Author Manuscript Author Manuscript Author Manuscript

REAGENT or RESOURCE	SOURCE	IDENTIFIER
Antibodies		
Rabbit polyclonal anti-A11	Abcam	Cat# ab126892; RRID: AB_11128526
Rabbit polyclonal anti-CDK1	Abcam	Cat# ab133327; RRID: AB_11155333
Sheep anti-DIG-Rhodamine, fab fragments	Sigma	Cat# 11207750910; RRID: AB_514501
Goat anti-rabbit AlexaFluor 488/555	ThermoFisher Scientific	Cat# A-11008/A-21428; RRID: AB_143165/ RRID: AB_141784
Chemicals, Peptides, and Recombinant Proteins		
Congo red	Sigma	75768
ANS	Sigma	A1028
Proteinase K, molecular biology grade	New England BioLabs	P8107S
1.4nm Nanogold negatively charged nanoparticles	Nanoprobes	2023
1.4nm Nanogold neutral nanoparticles	Nanoprobes	2010
ACM^{VHL} Short cationic domain: GTGRRIHSYRGHLWLF	This paper	N/A
β-amyloid Short cationic domain: DAEFRHDSGYEVHHQKL	This paper	N/A
ACM^{VHL} Short cationic domain – D mutant: GTGDDIHSYDGHLWLF	This paper	N/A
β-amyloid Short cationic domain – D mutant: DAEFDDDSGYEVDDQDL	This paper	N/A
R^4: RRRR	This paper	N/A
Critical Commercial Assays		
TRIzol	ThermoFisher Scientific	15596018
High-Capacity cDNA Reverse Transcription Kit	Applied Biosystems	4368814
PowerUp SYBR Green master mix	Applied Biosystems	A25780
pGEM-T Easy vector system	Promega	A1360
Illumina NextSeq 500 High Output kit	Illumina	FC-404–2004
Deposited Data		
Raw and analyzed data	This paper	GSE115731
Human reference genome NCBI Build 38, GRCh38	Genome Reference Consortium	https://www.ncbi.nlm.nih.gov/projects/genome/assembly/grc/human/
U13369 human ribosomal DNA unit	Pubmed	https://www.ncbi.nlm.nih.gov/nuccore/555853/
GL000220.1 human ribosomal DNA unit from GRCh38	Genome Reference Consortium	https://www.ncbi.nlm.nih.gov/projects/genome/assembly/grc/human/
BK000964.3 mouse ribosomal DNA unit	Pubmed	https://www.ncbi.nlm.nih.gov/nuccore/bk000964
Experimental Models: Cell Lines		
Human: MCF7 breast cancer cell line	ATCC	HTB-22
Oligonucleotides		
Primers for qPCR, see Table S1	This paper	N/A
RNA-FISH HC sequences, see Table S1	This paper	N/A
RNA-FISH $rIGS_{16}$RNA LC: 5'-DIG-AGGAA	This paper	N/A

Author Manuscript Author Manuscript Author Manuscript Author Manuscript

REAGENT or RESOURCE	SOURCE	IDENTIFIER
GGAGGGAAGGAAGGAAGGAAGGAAGG AAGGAAGGAAGGAAATAAA-DIG-3’		
RNA-FISH rIGS$_{22}$RNA LC1: 5’-DIG-TTTTC TTTCATTTTCTCTTTCTTTTCTTTTCTTTT TTTCTTTCTTGTATA-DIG-3’	This paper	N/A
RNA-FISH rIGS$_{22}$RNA LC2: 5’-DIG- ACAC AGAGAGAAAGACAGAGACGAACAGAGA GAAACAGACAGAGAGAAGG-DIG-3’	This paper	N/A
siRNA target sequences, see Table S1	This paper	N/A
In vitro RNA low complexity CU: 5’- UCUG UCUCUGUCUUUGUCUCUCUCUCCCC UCUCUGCCUGUCUCACUGUGUCUGUC UUCUGUCUUACUCUCUUUCUCUCCCC GUCUGUCUCUCUCUCUCU-3’	This paper	N/A
In vitro RNA low complexity AG: 5’-AGAGAG AGAGACAGAGAGAGACAGAGAGAGAGA GAGGAGGGAGAGAGAAAAAAGAAAGAAAA AAAGAAAAGAAAAGAAAGAGAAAAUGAAA GAAAAGG-3’	This paper	N/A
In vitro RNA high complexity #1: 5’-CCGGGAUUU CAGCCUUUAAAAGCGCGGGCCCUGCCACCUUU CGCUGUGGCCCUUACGCUCAGAAUGACGUGU CCUCUCUGCCGUAGGUUGACUCCUUGAG-3’	This paper	N/A
In vitro RNA high complexity #2: 5’-CCGGCCCGCC UGGUCUUCUGUCUCUGCGCUCUGGUGACCUCA GCCUCCCAAAUAGCUGGGACUACAGGGAUCUCU UAAGCCCGGGAGGGAGAGGUUAACG-3’	This paper	N/A
Recombinant DNA		
Plasmid: pFLAG-GFP	Audas et al., 2016	N/A
Plasmid: pEGFP-N1 TOPO™ Expression kit	ThermoFisher Scientific	K481001
Plasmid: pEGFP-C1 TOPO™ Expression kit	ThermoFisher Scientific	K482001
Software and Algorithms		
RNAfold		http://rna.tbi.univie.ac.at/cgi-bin/RNAWebSuite/RNAfold.cgi
ZipperDB for fibrillation propensity	Goldschmidt et al., 2010	https://services.mbi.ucla.edu/zipperdb/
Cutadapt (v1.15)		https://github.com/marcelm/cutadapt/
STAR (v2.3)		https://github.com/alexdobin/STAR
Samtools		http://samtools.sourceforge.net/
Integrative Genomics Viewer		http://software.broadinstitute.org/software/igv/